



HAL
open science

Evaluation of the acoustic radiation of contrasted orthogonally stiffened plates from homogenized model

Pascal Fossat, Thomas Brion, Mohamed Ichchou, Olivier Bareille

► To cite this version:

Pascal Fossat, Thomas Brion, Mohamed Ichchou, Olivier Bareille. Evaluation of the acoustic radiation of contrasted orthogonally stiffened plates from homogenized model. *Journal of Sound and Vibration*, 2023, 562, pp.117831. 10.1016/j.jsv.2023.117831 . hal-04588846

HAL Id: hal-04588846

<https://hal.science/hal-04588846>

Submitted on 27 May 2024

HAL is a multi-disciplinary open access archive for the deposit and dissemination of scientific research documents, whether they are published or not. The documents may come from teaching and research institutions in France or abroad, or from public or private research centers.

L'archive ouverte pluridisciplinaire **HAL**, est destinée au dépôt et à la diffusion de documents scientifiques de niveau recherche, publiés ou non, émanant des établissements d'enseignement et de recherche français ou étrangers, des laboratoires publics ou privés.

Evaluation of the acoustic radiation of contrasted orthogonally stiffened plates from homogenized model

Pascal Fossat^{a,*}, Thomas Brion^a, Mohamed Ichchou^a, Olivier Bareille^a

^a*Vibroacoustics and Complex Media Research Group VIAME, LTDS - CNRS UMR 5513, Centre Lyonnais d'Acoustique CeLyA, École Centrale de Lyon, Université de Lyon, France*

Abstract

This paper presents a study of the acoustic radiation from a ribbed plate with inner resonance. Based on explicit design rules and homogenized model for flexural waves, it reminds that bending wave propagation significantly differs from classical models in case of strong contrast between constituents, resulting into inner resonance. In order to demonstrate that this model advantageously supplements the Timoshenko orthotropic plate model, it links the atypical structural response on common vibroacoustic indicators, which are of value to discuss on different levels of abstraction. In either infinite or finite cases, the resulting indicators obtained from the homogenized model matches with classical trends outside frequency bands associated with local resonance, however inner resonance yields additional frequency ranges in which acoustic radiation is either strongly reduced or enhanced. For both mechanical and acoustic quantities, key indicators are successfully compared with classical theory for either poorly and highly contrasted ribbed plates in order to confirm the diversification of acoustic behaviors encompassed by the homogenized model.

Keywords: Homogenization, Contrasted structure, Ribbed plate, Inner resonance media, Acoustic radiation, Sound transmission loss

*Corresponding author

Email address: `pascal.fossat@ec-lyon.fr` (Pascal Fossat)

1 **Highlights**

- 2 • Homogenized model of ribbed plates discussed versus Timoshenko or-
3 thotropic model
- 4 • Benefit of homogenized model over classical model for highly contrasted
5 plates
- 6 • Theoretical influence of the locally resonant behavior on vibroacoustic
7 indicators

8 Introduction

9 The use of ribbed panels in aerospace or automotive engineering is wide
10 and the current trends associated with sound and vibration control have been
11 a vector of development of new models and methods. Indeed the coupled
12 problem of a vibrating plate in a fluid medium is related to fluid-structure
13 interaction for which assumptions can be made either on the dynamic be-
14 havior of the plate, the properties of the fluid governing the radiated field,
15 the nature of the coupling between the plate and the fluid.

16 The acoustic field radiated by a plate is known from its vibratory re-
17 sponse [1, 2]. The simple case of an infinite thin isotropic plate radiating in an
18 infinite fluid domain shows the existence of a critical frequency below which
19 the plate vibrates without radiating acoustic waves (subsonic regime with
20 evanescent waves), and above which the plate radiates plane waves whose di-
21 rection of propagation depends on the frequency (supersonic regime). While
22 the infinite case has some analytical solutions for both regimes, the determi-
23 nation of the acoustic field radiated in finite case requires the implementation
24 of the Rayleigh integral based on the Green kernel available for given set of
25 geometries. It is outlined that although the structural response of the plate
26 can be determined or approached analytically using Rayleigh-Ritz method,
27 virtual works principle, or by finite element or finite difference schemes, the
28 acoustical response is only accessible through the resolution of the Rayleigh
29 integral, that might be computationally expensive. For a complete review of
30 structure-borne acoustics of rectangular panels and comprehensive review of
31 numerical techniques to assess the low frequency radiation, one may respec-
32 tively refer to the papers from [3, 4]. This overview of methods provides a
33 reading grid for various experimental works in the scope of this paper, such
34 as those of [5, 6].

35 A key point of this paper is the aspect of contrast, which can be either
36 geometric or mechanical in nature. The modeling of this specific feature mod-
37 ifies the structure of the bi-laplacian operator (classical Kirchhoff's descrip-
38 tion) by introducing additional bending stiffness coefficients associated with
39 orthotropy. The most common model for orthotropic plate was developed
40 by Timoshenko [7] and applies to unidirectionally and orthogonally ribbed
41 plates, beam grids, corrugated plates through the calculation of equivalent
42 bending stiffness terms.

43 Focusing on ribbed plates, for which the orthotropic nature arises from
44 the arrangement of stiffeners on a bare plate, it appears that the stiffeners

45 significantly affect its dynamic characteristics. One must cite the pioneering
46 works of [8] who demonstrated that the radiation efficiency is increased below
47 the critical frequency by assuming stiffeners as regularly spaced supports. A
48 physical interpretation was introduced later in [9] and describes how the ribs
49 may bring wavenumbers from the subsonic regime to the supersonic regime.
50 Among the different theories to describe the dynamic behavior of periodic
51 stiffened panel, one may refer to the wavenumber based method [10], the
52 space-harmonic analysis [11], wave finite element method [12–14], and some
53 analytical approaches [15–17], among which homogenization is a relevant
54 theoretical framework for the construction of analytical models.

55 However, most of these works consider structures in which the mechanical
56 properties of the constituents are poorly contrasted. Particularly, these stud-
57 ies give either analytical results on weakly contrasted structures, or numerical
58 results on contrasted structures.

59 Among the analytical approaches, a benefit of periodic homogenization
60 is to upscale the physics from to micro-scale to the macro-scale without as-
61 sumption about the nature of the model to be found [18]. Also, giving that
62 the resonant nature at the macroscopic scale comes from the contrast be-
63 tween the constituents, the transition from weakly to strongly contrasted, *i.e.*
64 non-resonant to resonant, can be assessed. Indeed, the asymptotic homoge-
65 nization is capable of precisely describe this transition of behavior through
66 the scaling of geometrical and mechanical contrasts directly into the deriva-
67 tion process. In this way, on may cite the derivation of models of contrasted
68 frames [19], plate-type structures such as laminated plates [20, 21], unidirec-
69 tional ribbed plate [22], and orthogonally ribbed plates [23].

70 Although this analytical method is intrinsically limited to low frequen-
71 cies, it is sufficient to capture the first eigenmodes of the structure while
72 incorporating the effect of local resonance. As an example, the locally reso-
73 nant nature of an infinite unidirectional ribbed plate was briefly introduced
74 in [24] and showed that it brings additional frequency bands of radiation
75 below the critical frequency, as well as evanescent waves below the critical
76 frequency. Also, explicit design rules could allow to tune local resonance
77 onto the coincidence frequency as in [25] and thus make it possible to reach
78 improved sound insulation as already known for locally resonant mechanical
79 or acoustical metamaterials, and recently demonstrated by [26–28].

80 Although numerous study bring meaningful phenomenological interpreta-
81 tions on the radiation of resonant panels, only little attention has been paid
82 to draw a parallel between an analytical model of contrasted ribbed and its

83 acoustic radiation compared to classical model.

84 In this paper, the acoustic radiation of a contrasted orthotropic plate is
85 reported in the infinite case and finite case. The paper is organized into three
86 sections. A preliminary description of the structure under study is introduced
87 in section 1, together with the underlying physics and associated mechanisms.
88 The models introduced will be exploited in the case of an infinite plate,
89 then of finite dimensions. Particularly, section 2 presents the outputs of
90 the model on common vibroacoustic indicators such as radiation efficiency,
91 acoustic impedance, and transmission loss. The section 3 deals with finite
92 plate analysis, and compares the response of the contrasted model with that
93 of Timoshenko, in terms of mean square velocity and sound transmission
94 loss.

95 1. Physical insight of ribbed plate models

96 1.1. Structure under study

97 The periodic orthogonally ribbed plate hereafter called 2D-ribbed plates
98 under study is depicted in Fig. 1. It comprises identical "micro"-plate ele-
99 ments (denoted \mathcal{P}) connected to an orthogonal beam grid (denoted \mathcal{G}), both
100 made of isotropic elastic materials. The beams of the grid are assumed signif-
101 icantly stiffer than the internal plates. We focus on the dynamic range such
102 that the size of the cell (or the width of \mathcal{P}) is small compared to the wave-
103 length in the beam grid. The referential frame of unit vectors ($\mathbf{e}_x, \mathbf{e}_y, \mathbf{e}_z$) is
104 such that \mathbf{e}_x and \mathbf{e}_y are the in-plane vectors along the orthogonal ribs, while
105 \mathbf{e}_z is the out-of-plane vector. The beam grid \mathcal{G} is defined by perpendicular
106 beams. The stiffeners oriented along x (resp. y) are identical and regularly
107 spaced by the length ℓ_y (resp. ℓ_x).

108 Each segment of stiffeners between two consecutive nodes is modeled as an
109 Euler-Bernoulli beam (denoted $\mathcal{B}_x, \mathcal{B}_y$). The geometrical parameters of \mathcal{B}_j ,
110 with $j = x, y$, are (ℓ_j, h_j, b_j, A_j) which stand respectively for their length, \mathbf{e}_z -
111 thickness, width with $b_j = O(h_j)$ and section area $A_j = h_j b_j$. The mechanical
112 parameters $(E_j, I_j = b_j h_j^3 / 12, G_j, \mathcal{I}_j, \rho_j, \Lambda_j = \rho_j A_j, \rho_j J_j)$ denote respectively
113 the Young Modulus, the bending inertia, the torsional modulus and torsional
114 inertia, the density, the linear mass, and the polar moment. The dimensions
115 of the sections $\sqrt{A_j}$ are assumed small with respect to the lengths ℓ_j so
116 that the behavior of the inter-node elements can be effectively modeled as
117 Euler-Bernoulli beams. It is further assumed that the geometrical and the

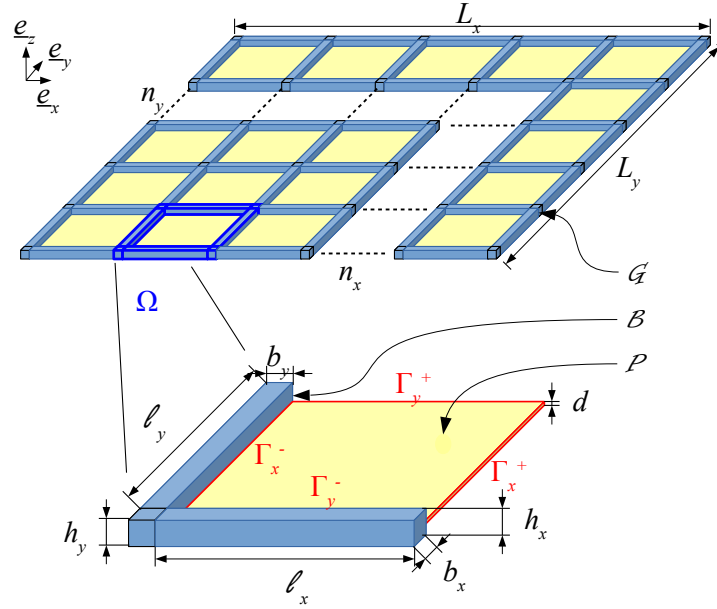


Figure 1: Orthogonally ribbed plate with with beams constituting the beam grid \mathcal{G} , and focus on the unit cell Ω made of micro-beams \mathcal{B} and internal micro-plate \mathcal{P}

118 mechanical parameters of both types of beams \mathcal{B}_j are of the same order of
 119 magnitude.

120 The material of the micro-plates \mathcal{P} of area $\ell_x \ell_y$ and thickness d , have a
 121 Young's modulus E_p , a Poisson's ratio ν_p and a density ρ_p . The corrected
 122 plate modulus is $E'_p = E_p / (1 - \nu_p^2)$. The plate bending inertia is denoted
 123 $I'_p = d^3 / 12$ and the surface mass $\Lambda'_p = \rho_p d$.

124

125 According to the ribbed plate illustrated in Fig. 1, two models are pre-
 126 sented in the following : a poorly contrasted ribbed plate in section 1.2 and
 127 a highly contrasted plate model in section 1.3.

128 1.2. Summary of the 2D ribbed plate model without contrasts

129 As introduced previously, numerous studies dealing with orthogonally
 130 ribbed plates are based on Timoshenko description [7]. This description is
 131 originally given in statics and is commonly extended in the dynamic regime

132 by introducing $-\omega^2\Lambda u$ on the right hand side of the equation. For an or-
 133 thotropic plate defined in the (x, y) plane, the equation governing its trans-
 134 verse displacement u takes the form of Eq. (1) with coefficients Eq. (2).

$$\left(D_x \frac{\partial^4}{\partial x^4} + D_y \frac{\partial^4}{\partial y^4} + 2D_{xy} \frac{\partial^4}{\partial x^2 \partial y^2} \right) u = \omega^2 \Lambda u \quad (1)$$

135 where the bending rigidities and mass are

$$D_x = \frac{E_x I_x}{l_y} + E'_p I_p; \quad D_y = \frac{E_y I_y}{l_x} + E'_p I_p; \quad D_{xy} = E'_p I_p; \quad \Lambda = \frac{\Lambda_x}{\ell_y} + \frac{\Lambda_y}{\ell_x} + \Lambda'_p \quad (2)$$

136 From the original description in statics, the expressions of respective
 137 bending stiffness suggest that the plate contributes to the global rigidity
 138 of the plate. This is understood since same order of magnitude, one cannot
 139 neglect the effect of the plate to the beam grid. Also, introducing $-\omega^2\Lambda u$
 140 on the right hand side of the equation without prior investigation might not be
 141 fully appropriated to capture all the frequency dependent phenomena.

142 Moving to the case of contrasted plate would require a decoupling of the
 143 beam grid and the plate, so that contrast is introduced in the plate either
 144 with geometrical or mechanical parameters. The next section introduces the
 145 contrast between the beam grid and the internal plates, and discusses how
 146 contrast enriches Timoshenko description.

147 *1.3. Summary of the homogenized ribbed plate model with contrasts*

148 This subsection defines favorable conditions for inner resonance and sum-
 149 marizes the derivation of the homogenized model. The homogenization pro-
 150 cess is carried out according to the following steps : *i*) the homogenization of
 151 periodic discrete media method enables to derive the dynamic model describ-
 152 ing the transverse vibration of the beam grid only, *ii*) the coupling between
 153 the beam grid and the internal plates is then introduced considering that
 154 the grid is loaded by efforts and moments exerted by the plates attached to
 155 it, *iii*) the calculation of the dynamic contribution of the resonant internal
 156 plates driven by the motion of the grid.

157 *1.3.1. Contrasts definition and design rules*

158 Inner resonance is defined so as the stiff orthogonal beam grid conveys
 159 the large wavelength, while the soft internal plate experiences a local reso-
 160 nance. Such a mixed regime within the cell results into *i*) an inhomogeneous

161 kinematics where the plate and grid displacements differ at the leading order
 162 and *ii*) an asymmetrical coupling where the grid forces the soft plate.

163 First, as for the co-dynamic condition, the beam grid \mathcal{G} and \mathcal{P} -plate
 164 fundamental resonances are of same order i.e., $O(\omega_{\mathcal{G}}) = O(\omega_p)$, so that :

$$O\left(\frac{E'_p I'_p}{\Lambda'_p \ell^4}\right) = O\left(\frac{EI}{\Lambda L^4}\right) \quad \text{i.e.} \quad \frac{E'_p \rho}{E \rho_p} = O\left(\frac{h^2 \ell^4}{d^2 L^4}\right) = O\left(\varepsilon^4 \frac{h^2}{d^2}\right) \quad (3)$$

165 This relation highlights the significant contrasts of mechanical properties of
 166 the constituting materials of the beam grid \mathcal{G} and \mathcal{P} -plate.

167 Second, as for the asymmetric coupling, the grid acts as the forcing system
 168 that imposes its displacement to the internal plate which bring forces back on
 169 the grid. Such a coupling between the transverse balance of the grid loaded
 170 by the internal plates requires :

$$\text{div}(\mathbf{T}_{\mathcal{G}}) = O(T_p) \quad (4)$$

171 where $\mathbf{T}_{\mathcal{G}}$ relates to the transverse shear force (unit kN) in the grid \mathcal{G} and
 172 T_p is the transverse linear shear force in the internal \mathcal{P} -plate (unit kN/m).

173 Thus, from Eq. (4) and recalling that $b_k = O(h_k)$ one deduces the follow-
 174 ing requirement

$$O\left(E \frac{bh^3}{L^4}\right) = O\left(E'_p \frac{d^3}{\ell^3}\right) \quad \text{i.e.} \quad \frac{E'_p}{E} = O\left(\frac{\ell^3 \ell^4}{d^3 L^4}\right) = O\left(\varepsilon^4 \frac{h^2}{d^2}\right) \quad (5)$$

175 In practice, $\rho/\rho_p = O(1)$ and the two conditions Eq. (3) and Eq. (5)
 176 reduce to $\frac{E'_p}{E} = O\left(\varepsilon^4 \frac{h^2}{d^2}\right)$. For ribbed plate made of a single material $E'_p =$
 177 E , and the inner-resonance arises when $d/h = O(\ell^2/L^2)$, i.e. for plates \mathcal{P}
 178 significantly thinner than the beams of the grid \mathcal{G} . If the plates material
 179 is much softer than the grid material, namely $E'_p = O(\varepsilon^4 E)$ then $d/h =$
 180 $O(\ell/L)$ enables the inner-resonance to occur. Note that in these realistic
 181 cases, the bending stiffness of the plate is much smaller than that of the grid,
 182 in accordance with the asymmetry of the coupling. The case of inverted
 183 material properties so that the plate exhibits stiff properties and beam grid
 184 soft properties is not assessed here.

185 1.3.2. Homogenized formulation of the flexural behavior

186 Starting with the beam grid, the up-scaling process is performed through
 187 HPDM method (namely Homogenization of Periodic Discrete Media). The

188 developments proceed into three steps, namely, the discretization of the dy-
189 namic balance, then the homogenization procedure itself through scale sepa-
190 ration assumption and normalization, leading to the continuous model from
191 the discrete pattern. This method applies under the key assumption of scale
192 separation. This means that the wavelength $O(L)$ is much larger than the
193 period size $O(l)$ and consequently $\epsilon = l/L \ll 1$. The macroscopic descrip-
194 tion of the grid, valid at the dominant order, is the limit behavior reached
195 for $\epsilon = l/L \rightarrow 0$. After these few steps, we are left with the following
196 macroscopic description of the grid at the leading order :

$$\left\{ \begin{array}{l} \operatorname{div}(\mathbf{T}^{\mathcal{G}}) + \omega^2 \Lambda^{\mathcal{G}} u = 0 \quad ; \quad \Lambda^{\mathcal{G}} = \frac{\Lambda_x}{\ell_y} + \frac{\Lambda_y}{\ell_x} \\ \operatorname{div}(\mathbf{M}^{\mathcal{G}}) - \mathbf{T}^{\mathcal{G}} - \omega^2 \mathbf{J}^{\mathcal{G}} \cdot \mathbf{grad}(u) = 0 \\ \mathbf{M}^{\mathcal{G}} = - \left(\begin{array}{cc} \frac{E_x I_x}{\ell_y} \partial_x^2 u & \frac{G_y J_y}{\ell_x} \partial_x \partial_y u \\ \frac{G_x J_x}{\ell_y} \partial_y \partial_x u & \frac{E_y I_y}{\ell_x} \partial_y^2 u \end{array} \right) \quad ; \quad \mathbf{J}^{\mathcal{G}} = \left(\begin{array}{cc} \rho_y J_y & 0 \\ 0 & \rho_x J_x \end{array} \right) \end{array} \right. \quad (6)$$

197 The governing equation Eq. (6) may be written under condensed form

$$\begin{aligned} \frac{E_x I_x}{\ell_y} \frac{\partial^4 u}{\partial x^4} + \frac{E_y I_y}{\ell_x} \frac{\partial^4 u}{\partial y^4} + \left(\frac{G_x I_x}{\ell_y} + \frac{G_y I_y}{\ell_x} \right) \frac{\partial^4 u}{\partial x^2 \partial y^2} \\ + \omega^2 \left(\frac{\rho_y J_y}{\ell_x} \frac{\partial^2 u}{\partial x^2} + \frac{\rho_x J_x}{\ell_y} \frac{\partial^2 u}{\partial y^2} \right) = \omega^2 \left(\frac{\Lambda_x}{\ell_y} + \frac{\Lambda_y}{\ell_x} \right) u \end{aligned} \quad (7)$$

198 The governing equation Eq. (6) shows the coupling between the flexural
199 and torsional behaviors. Note that in statics ($\omega \rightarrow 0$), this model already
200 differs to that of Timoshenko Eq. (1). Note also that the inertial term con-
201 taining the polar moments $\mathbf{J}^{\mathcal{G}}$ may be neglected in regards to those related to
202 the linear masses $\Lambda^{\mathcal{G}}$. Note finally that an additional inertial effect following
203 comment made in section 1.2.

204 The action of internal plates is then introduced in the beam grid model
205 in the form an external loading constituted by a shear force \mathcal{F} and a couple
206 \mathcal{C} resulting from the contact forces. The rigorous calculation of these terms
207 is detailed in [23]. Calculating analytically these terms yield the effective
208 model of the 2D ribbed plate that describes the grid behavior enriched by

209 for the locally resonant internal plates:

$$\begin{cases} \operatorname{div}(\mathbf{T}^{\mathcal{G}}) + \omega^2(\Lambda^{\mathcal{G}} + \Lambda'_p \langle \phi_\omega \rangle)u = 0 \\ \operatorname{div}(\mathbf{M}^{\mathcal{G}}) - \mathbf{T}^{\mathcal{G}} - \omega^2 \mathbf{J}^{\mathcal{G}} \cdot \mathbf{grad}(u) = 0 \end{cases} \quad (8)$$

210 with $\mathbf{M}^{\mathcal{G}}$ and $\mathbf{J}^{\mathcal{G}}$ as defined in Eq. (6). Note also that the description could
 211 be improved by considering the correction factors constituted by the higher
 212 order terms of the asymptotic process. These could be relevant in case scale
 213 separation is not fulfilled. The inner resonance effect appears in Eq. (8)
 214 through the frequency dependent effective parameter $\langle \phi_\omega \rangle$, associated with
 215 the dynamic motion of the internal plate. This results into a non conventional
 216 apparent mass term whose determination is performed by integrating the
 217 transverse displacement of the internal plate over its surface. Since there
 218 is no analytical expression of this quantity for a square clamped plate, the
 219 latter is approximated by that of a clamped circular plate. This provides an
 220 approximated value, denoted $\langle \phi_\omega^c \rangle$, for a square plate of side l by matching
 221 its first eigenfrequency with that of an equivalent circular plate of radius a .
 222 The corresponding approximation reads:

$$\langle \phi_\omega \rangle \approx \langle \phi_\omega^c \rangle = \frac{4}{\delta a} \frac{I_1(\delta a) J_1(\delta a)}{I_1(\delta a) J_0(\delta a) + I_0(\delta a) J_1(\delta a)} \quad (9)$$

223 where $a \approx 0.53l$ is the equivalent radius, J_k and I_k are the Bessel and modified
 224 Bessel functions of the first/second kind, δ is the wavenumber such that
 225 $\delta^4 = \Lambda'_p \omega^2 / E'_p I_p$. The denominator of Eq. (9) is the transcendental equation
 226 whose roots δa are used to calculate the eigenfrequencies of the circular plate.
 227 The matching is performed on the first mode, and determines the radius of
 228 the equivalent circular plate, that is $a = 0.53l$. Although this reasoning is
 229 empirical and based on the resemblance of the first mode shapes of a square
 230 and circular plate, this estimate perfectly fits the first resonance but over-
 231 predicts the eigenfrequency of the second mode with an error of 5%. (see
 232 [23]).

233 The properties of $\langle \phi_\omega \rangle$ are such that $\langle \phi_\omega \rangle \rightarrow 1$ as $\delta \rightarrow 0$ which means that
 234 the effective mass is the real static mass, and $\langle \phi_\omega \rangle \rightarrow \pm\infty$ as $I_1(\delta a) J_0(\delta a) +$
 235 $I_0(\delta a) J_1(\delta a) = 0$, which roots corresponds to the plate's eigenfrequencies.

236

237 *1.3.3. Dispersion features*

238 Assuming an harmonic bending wave in the form $u(\mathbf{x}) = \exp(ik_\theta \mathbf{n}_\theta \cdot \mathbf{x})$
 239 propagating in the direction $\mathbf{n}_\theta = \cos \theta \mathbf{e}_x + \sin \theta \mathbf{e}_y$. Taking into account the
 240 facts that the terms associated with polar moments \mathbf{J}^G are of weak magnitude
 241 compared to the translational inertia, this term can be disregarded at the
 242 leading order. Consequently, the bending wavenumber $k_\theta(\omega)$ is given by :

$$k_\theta^4 \left(\frac{E_x I_x}{\ell_y} \cos^4 \theta + \frac{E_y I_y}{\ell_x} \sin^4 \theta + \left(\frac{G_x \mathcal{I}_x}{\ell_y} + \frac{G_y \mathcal{I}_y}{\ell_x} \right) \cos^2 \theta \sin^2 \theta \right) - \omega^2 (\Lambda^G + \Lambda'_p \langle \phi_\omega \rangle) = 0 \quad (10)$$

243 The inner resonance contained in $\langle \phi_\omega \rangle$ leads to dispersion features that differs
 244 distinctly from the classical bending case in which $k \propto \sqrt{\omega}$ in the whole
 245 frequency range. Significant changes are expected in the neighborhood of the
 246 internal plate's eigenmodes. Wavenumbers will be the subject of a special
 247 discussion in the section 2.1.

248 *1.4. Concluding remarks*

249 As an extension to the classical orthotropic plate equation Eq. (1) with
 250 coefficients Eq. (2) proposed by Timoshenko, homogenization introduces a
 251 dynamic description taking into account contrast between the beam and
 252 internal plates. Such an extended formulation is found as :

$$\frac{E_x I_x}{\ell_y} \frac{\partial^4 u}{\partial x^4} + \frac{E_y I_y}{\ell_x} \frac{\partial^4 u}{\partial y^4} + \left(\frac{G_x \mathcal{I}_x}{\ell_y} + \frac{G_y \mathcal{I}_y}{\ell_x} \right) \frac{\partial^4 u}{\partial x^2 \partial y^2} + \omega^2 \left(\frac{\rho_y J_y}{\ell_x} \frac{\partial^2 u}{\partial x^2} + \frac{\rho_x J_x}{\ell_y} \frac{\partial^2 u}{\partial y^2} \right) = \omega^2 (\Lambda^G + \Lambda_p \langle \phi_\omega \rangle) u \quad (11)$$

253 Remarking that the terms associated with polar moments are of weak
 254 magnitude compared to the inertia, this term can be neglected at the leading
 255 order, so that Eq. (11) degenerates into

$$\left(D_x \frac{\partial^4}{\partial x^4} + D_y \frac{\partial^4}{\partial y^4} + 2D_{xy} \frac{\partial^4}{\partial x^2 \partial y^2} \right) u = \omega^2 (\Lambda^G + \Lambda_p \langle \phi_\omega \rangle) u \quad (12)$$

256 where the bending stiffness and mass are

$$D_x = \frac{E_x I_x}{\ell_y} ; D_y = \frac{E_y I_y}{\ell_x} ; D_{xy} = \frac{G_x \mathcal{I}_x}{\ell_y} + \frac{G_y \mathcal{I}_y}{\ell_x} ; \Lambda^G = \frac{\Lambda_x}{\ell_y} + \frac{\Lambda_y}{\ell_x} \quad (13)$$

257 From Eq. (11) with coefficients Eq. (13), two important observations are
 258 made. First, the structure of the differential operation changes in such a
 259 way it still contains the bi-laplacian operator and includes additional terms
 260 of bending and torsional stiffness with rotational inertia. Second, the refer-
 261 ence equation Eq. (1) with coefficients Eq. (2) no longer considers the plate
 262 contribution in the elastic part, but in the inertial part. The plate is no
 263 longer contained in the bending stiffness. This is fully consistent with the
 264 fact that a contrasted ribbed plate will exhibit a dynamic behavior mostly
 265 governed by the grid, and the internal plates will affect the global response
 266 only around frequency bands in which their dynamic behavior differs from
 267 that of the grid.

268 From this introduction on the mechanical part, the sound radiation from
 269 plates can be modeled assuming it is either infinite or finite. The next two
 270 sections 2 and 3 are respectively dedicated to infinite and finite cases.

271 **2. Acoustic radiation - Infinite case**

272 This section presents an investigation onto a infinite ribbed plate. In
 273 anticipation of an experimental investigation, the dimensions of the internal
 274 plates are calculated so as to correspond to a feasible plate. Two designs
 275 are obtained : first is denoted \mathcal{R}_1^∞ , and is associated with geometrical and
 276 mechanical contrast between the grid and internal plate considering the ribs
 277 are identical in the two directions, second is denoted \mathcal{R}_2^∞ , and introduces
 278 stiffeners of different dimensions in the two directions, in order to better ex-
 279 hibit the orthotropic nature of the plate. According to the indicators defined
 280 in section 2.1, as well as the geometrical parameters and mechanical proper-
 281 ties given in Table 1, Table 2, the investigation will be expanded in terms of
 282 radiation efficiency (section 2.2) and transmission loss (section 2.3).

283 *2.1. Methods and chosen sets of parameters*

284 As for the methods, let consider an infinite plate with incident acous-
 285 tic plane wave, as illustrated in Fig. 2. The expressions the transmission
 286 coefficient is derived from *i*) the acoustic pressure of the incident, reflected
 287 and transmitted waves, *ii*) the pressure difference on both face of the plate
 288 combined with *iii*) the continuity of pressure and velocity at the fluid-solid
 289 interface.

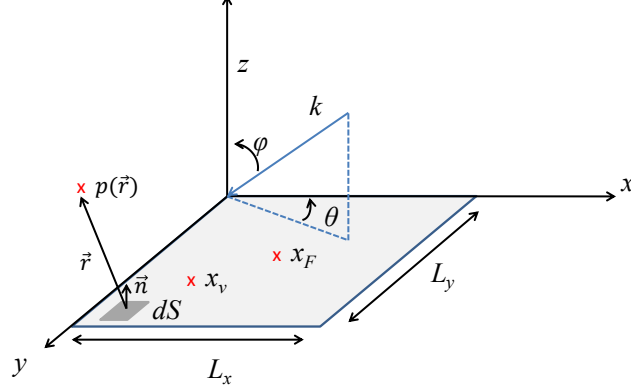


Figure 2: Notations used for the sound radiation investigation : ribbed plate in the (x, y) plane, angle of incident plane wave ϕ , azimuth angle θ of wave propagating in the plate. Location of point force x_F and observation point x_v for calculation of structural response. Elementary radiating surface dS with normal direction \mathbf{n} towards receiver point.

290 Let us consider an infinite orthotropic plate driven by an incident pressure
 291 $p(x, y, z)$ which governing equation is :

$$\left(D_x \frac{\partial^4}{\partial x^4} + D_y \frac{\partial^4}{\partial y^4} + 2D_{xy} \frac{\partial^4}{\partial x^2 \partial y^2} \right) u - \omega^2 \Lambda u = p(x, y, z) \quad (14)$$

292 When the pressure field is supposed of the form of an incident plane wave
 293 with a wavenumber $k = \omega/c_0$, an incidence angle ϕ and an azimuth angle
 294 θ . In this case, the incidence angle ϕ is the angle between the wave vector
 295 and the normal direction to the plate, and the azimuth angle θ gives its
 296 orientation in the plane of the plate. As for the incident plane wave, we state
 297 $p(x, y, z)$ as:

$$p(x, y, z) = p_0 \exp(-i(k_x x + k_y y + k_z z)) \quad (15)$$

298 with $k_x = k \sin \phi \cos \theta$, $k_y = k \sin \phi \sin \theta$, $k_z = k \cos \phi$ are the acoustic
 299 wavenumbers in the different directions.

300 On the surface of the plate, $p(x, y, z = 0) = p_0 \exp(-i(k_x x + k_y y))$, the
 301 transverse displacement on the plate, solution of the equation Eq. (14) is
 302 searched with the form:

$$u(x, y) = U \exp(-ik \sin \phi (\cos \theta x + \sin \theta y)) \quad (16)$$

303 The ratio between the acoustic pressure to the velocity of the plate is intro-
 304 duced as the surface impedance $Z_s = p/v = p/i\omega u$.

305 The forms of the pressure and the displacement are the same as for the
 306 infinite isotropic plate but in case of orthotropic plate, due to the angle
 307 dependence of the flexural wavenumber k_p , the relation becomes

$$(D_x \cos^4 \theta + D_y \sin^4 \theta + 2D_{xy} \cos^2 \theta \sin^2 \theta)(k^4 \sin^4 \phi - k_p^4(\theta))u = p \quad (17)$$

308 and therefore, the surface impedance is defined by:

$$Z_s(\theta, \phi) = \frac{-i}{\omega} (D_x \cos^4 \theta + D_y \sin^4 \theta + 2D_{xy} \cos^2 \theta \sin^2 \theta) (k^4 \sin^4 \phi - k_p^4(\theta)) \quad (18)$$

309 Due to the orthotropic nature of plate, and thus the existence of two
 310 critical frequencies, the coincidence frequency band exhibiting a typical gap
 311 becomes broader and smoother. A relatively small difference between the
 312 bending rigidity of stiffeners produces a small difference between their respec-
 313 tive critical frequencies. As the difference of stiffness increases, the critical
 314 frequencies might be separated by one or two orders of magnitude.

315 From this observation, the usual expression of surface impedance Z_s in-
 316 cludes these two critical frequencies, whose depend not only on the angle of
 317 incidence ϕ of the incident plane wave, but also on the azimuth angle θ in
 318 the plane of the plate (see Fig. 2). The surface impedance of the orthotropic
 319 plate is thus :

$$Z_s = j\omega\Lambda \left(1 - \left(\frac{f}{f_{c,x}} \cos^2 \theta + \frac{f}{f_{c,y}} \sin^2 \theta \right)^2 \sin^4 \phi \right) \quad (19)$$

320 For a given angle of incidence ϕ , the transmission coefficient τ is defined
 321 by :

$$\tau_{(\phi,\theta)} = \frac{1}{\left| \frac{Z_s}{2Z_0} + 1 \right|^2} \quad (20)$$

322 with $Z_0 = \rho_0 c_0 / \cos \phi$ the normal impedance of the fluid and Z_s the surface
 323 impedance of the plate. The calculation of this transmission coefficient in
 324 diffuse field conditions is performed by integrating Eq. (20) over all angles
 325 of incidence. Assuming plane wave incidence uniformly distributed over all
 326 angles, the statistical transmission factor is :

$$\tau_d = \frac{2}{\pi} \int_0^{\pi/2} \left(2 \int_0^{\pi/2} \tau_{(\phi,\theta)} \cos \phi \sin \phi d\phi \right) d\theta \quad (21)$$

327 Introducing finally τ as Eq. (20), the diffuse field transmission coefficient
 328 is formulated as :

$$\tau_d = \frac{2}{\pi} \int_0^{\pi/2} \int_0^1 \frac{d(\sin^2 \phi) d\theta}{\left| \frac{Z_s}{2Z_0} + 1 \right|^2} \quad (22)$$

329 In the following, the evaluation of this term is performed numerically. In
 330 addition to the transmission coefficient, the reduction index R is introduced
 331 as $R = -10 \log(\tau_d)$.

332

333 According to the design rules favorable to inner resonance presented above
 334 and considering a feasibility criterion, two designs are obtained : first is de-
 335 noted \mathcal{R}_1^∞ , and is associated with geometrical and mechanical contrast be-
 336 tween the grid and internal plate considering the ribs are identical in the
 337 two directions, second is denoted \mathcal{R}_2^∞ , and introduces stiffeners of different
 338 dimensions in the two directions. The geometrical parameters and mechan-
 339 ical properties are respectively given in Table 1 and Table 2. The models
 340 use hysteretic damping ratio introduced as an imaginary part of the Young's
 341 modulus $E = E(1 + i\eta)$, with $\eta = 1\%$ for aluminium and 5% for perspex.

Table 1: Geometrical parameters and mechanical properties associated with the 2D infinite ribbed plate \mathcal{R}_1^∞ .

$n_x = n_y = \infty$	E (GPa), ν	ρ (kg/m ³)	Dimensions (m)
Beam grid	$E_b=69$; $\nu_b = 0.3$	$\rho_b=2700$	$h_x = h_y = 1.5 \cdot 10^{-2}$ $b_x = b_y = 1.5 \cdot 10^{-2}$
Internal plates	$E_p=2$; $\nu_p = 0.37$	$\rho_p=1200$	$l_x = l_y = 7 \cdot 10^{-2}$ $d = 3 \cdot 10^{-3}$

342 Following the design \mathcal{R}_1^∞ in Table 1, the exact critical frequency is the
 343 same in both directions $f_{c,j} = \frac{c^2}{2\pi} \sqrt{\frac{\lambda_j + \lambda_p D \langle \phi_\omega \rangle}{D_j}}$. The first resonance frequency
 344 of the internal plate is $f_1^r = 1386$ Hz.

345 Following the design \mathcal{R}_2^∞ in Table 2, the exact critical frequencies in
 346 both directions $f_{c,j} = \frac{c^2}{2\pi} \sqrt{\frac{\lambda_j + \lambda_p D \langle \phi_\omega \rangle}{D_j}}$ could be estimated numerically. As
 347 an approximation, out of the inner resonance frequency bands, this critical

Table 2: Geometrical parameters and mechanical properties associated with the 2D infinite ribbed plate \mathcal{R}_2^∞ .

$n_x = n_y = \infty$	E (GPa), ν	ρ (kg/m ³)	Dimensions (m)
Beam grid	$E_b=69$; $\nu_b = 0.3$	$\rho_b=2700$	$h_x = 1.10^{-2}$, $h_y = 0.75 \cdot 10^{-2}$ $b_x = b_y = 1.10^{-2}$
Internal plates	$E_p=2$; $\nu_p = 0.37$	$\rho_p=1200$	$l_x = l_y = 7.6 \cdot 10^{-2}$ $d = 3 \cdot 10^{-3}$

348 frequency is bounded by that of a simple plate radiating in half-space $f_c^- =$
349 $\frac{c^2}{2\pi} \sqrt{\frac{\lambda_b}{D_x}}$, that is $f_c^- = 1613$ Hz as the lower bound, and will not be greater
350 than that of the rib and internal plate at rest $f_{c,j}^+ = \frac{c^2}{2\pi} \sqrt{\frac{\lambda_j + \lambda_p}{D_j}}$, that is
351 $f_{c,x}^+ = 2520$ Hz as the upper bound. This can be systematically verified. The
352 same observation is valid for the other direction, respectively $f_{c,y}^- = 2520$ Hz,
353 and $f_{c,y}^+ = 3323$ Hz. Also, the first resonance frequency of the internal plate
354 is $f_1^r = 1190$ Hz, and the second resonance frequency is $f_2^r = 3261$ Hz.

355 The effective mass $\langle \phi_\omega \rangle$ associated to internal for both design is plotted
356 in Fig. 3 for both designs. The trends observed is consistent with the be-
357 havior with the comment provided along Eq. (9), where the two resonance
358 frequencies clearly appear.

359 From Fig. 4, it can be shown that due to inner resonance, the flexu-
360 ral wavenumber, calculated from Eq. (10), can significantly vary below and
361 above the critical frequency. Classical results of acoustic radiation below and
362 above the critical frequency can be obtained for 60 Hz and 900 Hz respec-
363 tively. However, in case of inner resonance, the flexural wavelength can be
364 significantly greater than acoustic wavelength below the critical frequency,
365 giving rise to unconventional acoustic radiation. Alternatively, the flexu-
366 ral wavelength can be significantly lower than acoustic wavelength above
367 the critical frequency, giving rise to unconventional generation of evanescent
368 acoustic waves.

369 2.2. Radiation efficiency

370 An usual indicator to evaluate if a vibrating surface is a good sound
371 radiator is the radiation efficiency denoted σ defined in terms of wavenumbers

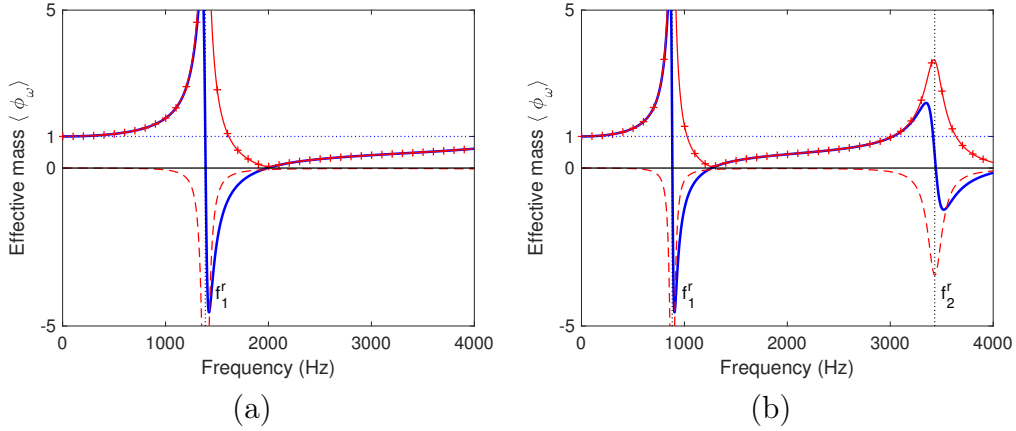


Figure 3: Dimensionless effective mass ϕ_ω associated with one single internal plate : real part (—), imaginary part (---), modulus (-+-), normalized static mass $y = 1$ (···). For plate \mathcal{R}_1^∞ (a) and plate \mathcal{R}_2^∞ (b).

372 as $\sigma = 1/\sqrt{1 - k_p^2/k^2}$. In this formula, we assume $k_p < k$; when the flexural
 373 wavelength in the plate increases with respect to the acoustic wavelength in
 374 air, the radiation efficiency tends to 1. The radiation efficiency is illustrated
 375 in Fig. 5 for both designs introduced above. As for the plate \mathcal{R}_1^∞ , for which
 376 stiffeners are identical in both directions, σ is the same for $\theta = 0$ or $\pi/2$,
 377 and the tuning of the inner resonance frequency onto the critical frequency
 378 decreases significantly the radiation factor in this region where the plate
 379 is known to be acoustically transparent. As for the plate \mathcal{R}_2^∞ , for which
 380 stiffeners are different in both directions, σ is illustrated for $\theta = 0$ and $\theta = \pi/2$
 381 and the influence of resonance frequencies is exhibited.

382 Radiation efficiency is an indicator for observing a preliminary manifesta-
 383 tion of the local resonance effect. It gives an indication of the behavior in
 384 the main directions of orthotropy. A global description obtained from an in-
 385 tegration on all angles, in the plate and in the air is proposed in the following
 386 section.

387 2.3. Sound transmission loss

388 2.3.1. Results for a single incidence angle

389 Two incidence angle are considered here for the acoustic wave reaching
 390 the plate : normal incidence condition $\phi = 0$, oblique incidence condition
 391 $\phi = \pi/3$.

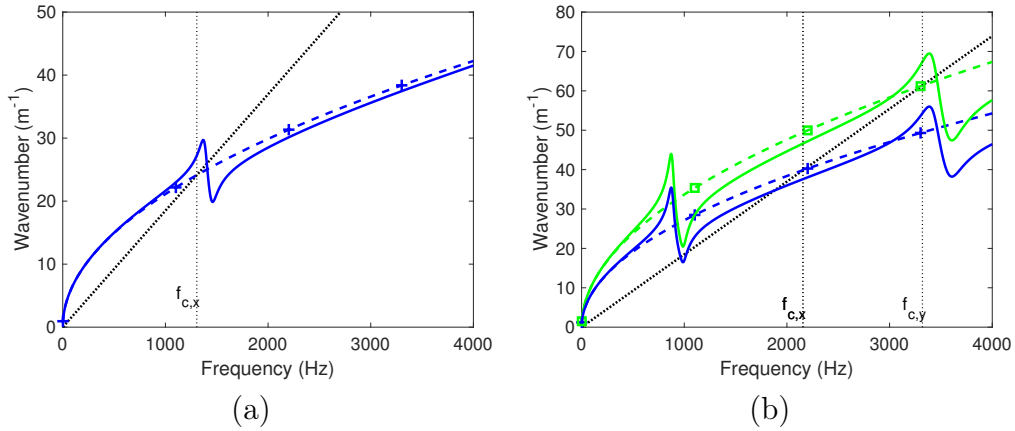


Figure 4: Flexural wavenumber in the x - and y - direction without inner resonance (resp. $(-+ -)$ and $(-\square-)$) and with inner resonance (resp. $(-)$, $(-)$), acoustic wavenumber in air (\cdots), and vertical dotted lines located at crossings indicated critical frequencies. For plate \mathcal{R}_1^∞ (a) and plate \mathcal{R}_2^∞ (b).

392 As for the normal incidence condition, Eq. (18) simplifies so as elastic ef-
 393 fects vanish and only inertial effect remain, that is consistent with the mass
 394 law approximation, which gives a quite appropriate description for frequen-
 395 cies lower than the critical frequency. The normal incidence transmission loss
 396 is illustrated for the two design in Fig. 6.

397 As for the oblique incidence, an arbitrary angle for the propagating wave
 398 in the plate is chosen as $\theta = \pi/3$. After passing the coincidence frequency,
 399 the transmission loss exhibits strong frequency dependence and the bending
 400 stiffness (elastic effects) becomes predominant over the mass law. This ef-
 401 fect is illustrated in Fig. 7 for 3 values of incidence angle, which shows that
 402 the classic trends are correctly recovered, *i.e.* the coincidence frequency de-
 403 creases as the angle of incidence get closer to the grazing incidence, and that
 404 the introduction of local resonance is perceptible in specific interval without
 405 modified the change of slope below and above the coincidence frequency.

406 To extend these results to diffuse field, one may integrate over all possi-
 407 ble incidence angles ϕ of the acoustic wave in air and possible directions of
 408 propagation θ of bending wave in the plate. The limits of the domains of
 409 integration are withdrawn since they correspond to grazing incidences and
 410 can give numerical errors.

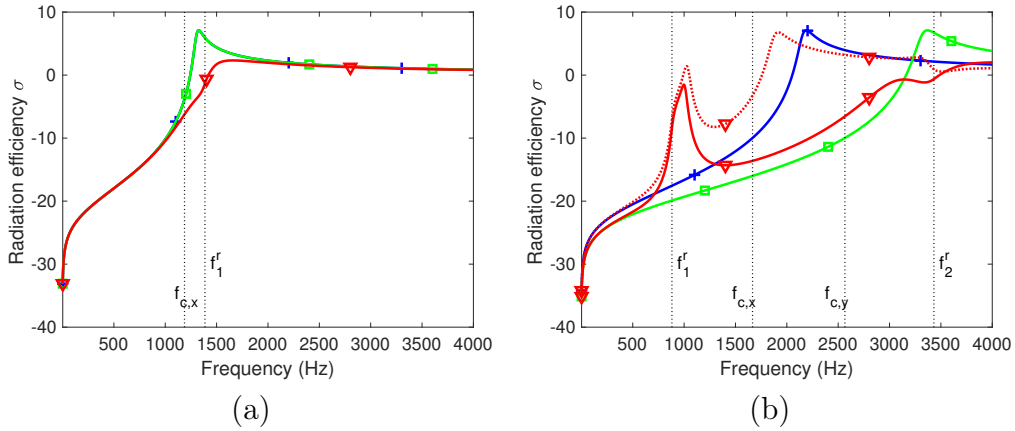


Figure 5: Radiation efficiency of orthotropic plate with inner resonance for $\theta = \pi/2$ ($-\triangle-$), $\theta = 0$ ($\cdots\triangle\cdots$), equivalent isotropic plate in x - direction ($-+ -$) and y - direction ($-\square-$). For plate \mathcal{R}_1^∞ (a) and plate \mathcal{R}_2^∞ (b).

411 *2.3.2. Results in diffuse field conditions*

412 The transmission loss is now calculated for the two designs. For each
 413 design, the transmission loss of the plate considering inert internal plates and
 414 the plate with the dynamic of the internal plates is plotted to best evidence
 415 the local resonance.

416 As for the design of the ribbed plate \mathcal{R}_1^∞ given in Table 1, the diffuse field
 417 transmission loss clearly shows the coincidence frequency of the equivalent
 418 isotropic plate in the x - direction and the plate at rest. The small shift
 419 in coincidence frequency is due to the increase of mass. However the most
 420 noticeable effects lies in the increase of transmission loss around the coinci-
 421 dence frequency. Minor fluctuations visible at high frequency are due to the
 422 discretization of the angle interval and are not related with inner resonance.

423 As for the design of the ribbed plate \mathcal{R}_2^∞ given in Table 2. Several quan-
 424 tities are illustrated, namely, the transmission loss associated with the equiv-
 425 alent isotropic plate along x - and y -, that associated with the orthotropic
 426 plate without inner resonance (disabling the frequency dependent term in
 427 Eq. (11), that is $\langle\phi_\omega\rangle = 1$), and that including the local resonance. Compar-
 428 ison is shown in Fig. 8 and shows the two critical frequencies associated with
 429 the equivalent isotropic plates along $-x$ and $-y$, since these have different
 430 bending stiffness in the two directions. A relatively small difference between
 431 rigidities produces a small difference between critical frequencies. The ribs
 432 increase the bending stiffness but lowers the critical frequency. This may

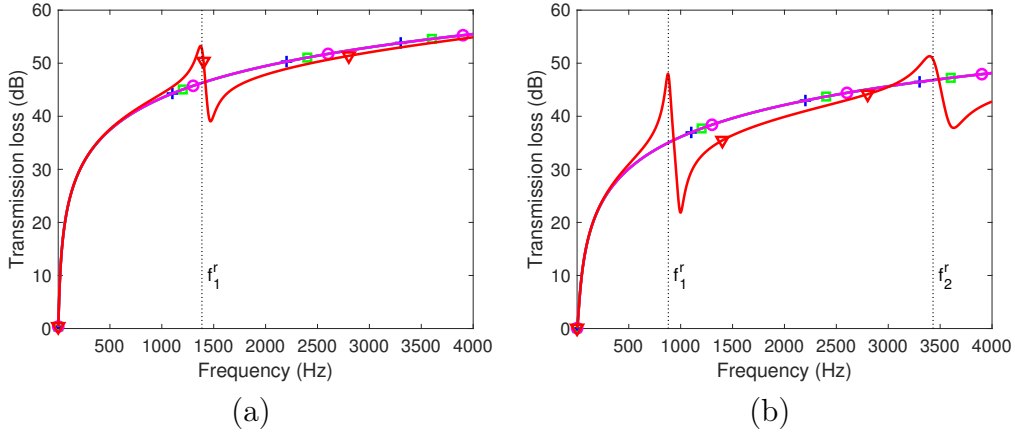


Figure 6: Normal incidence transmission loss of orthotropic plate with inner resonance ($-\nabla-$), plate at rest ($-\circ-$), equivalent isotropic plate in x - direction ($-\oplus-$) and y - direction ($-\square-$). For plate \mathcal{R}_1^∞ (a) and plate \mathcal{R}_2^∞ (b).

433 lead to an increased transparency in the useful frequency range. However,
 434 the locally resonant nature can be put to good use since it provides an addi-
 435 tional mechanism of attenuation in some frequency bands. In this way, the
 436 transmission loss of the orthotropic plate exhibits a dip between the afore-
 437 mentioned critical frequencies. When introducing the resonance of internal
 438 plates, additional fluctuations related to eigenmodes of the vibrating inter-
 439 nal plates contribute to the increase or decrease of transmission loss at their
 440 corresponding frequencies.

441 2.4. Concluding remarks on infinite case

442 This section introduced the relevant quantities to look at when investi-
 443 gating the radiation of plates Two realistic designs are obtained : first is
 444 associated with geometrical and mechanical contrast between the grid and
 445 internal plate, second introduces different stiffeners in the two directions, in
 446 order to better exhibit the orthotropic nature of the plate, still with inner
 447 resonance. Preliminary examination of wavenumbers suggests that in case
 448 of inner resonance, the flexural wavelength can be greater than the acous-
 449 tic wavelength below the critical frequency, giving rise to acoustic radiation,
 450 and alternatively, it can be lower than acoustic wavelength above the criti-
 451 cal frequency, giving rise to unconventional generation of evanescent acoustic
 452 waves. This is then confirmed by the observation of radiation efficiency,
 453 which shows that tuning the inner resonance frequency around the critical

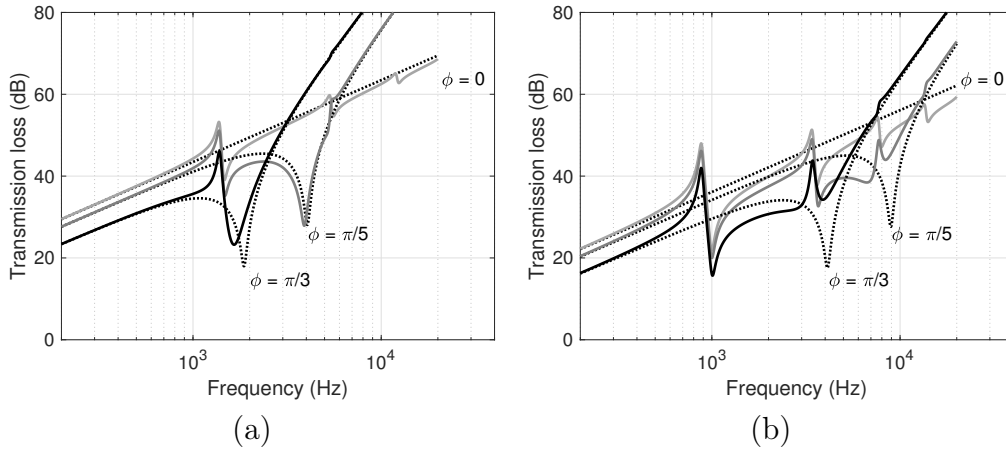


Figure 7: Oblique incidence transmission loss of orthotropic plate with inner resonance (—), plate at rest (⋯), for $\phi = 0, \pi/5, \pi/3$, from light to dark grey. For plate \mathcal{R}_1^∞ (a) and plate \mathcal{R}_2^∞ (b).

454 frequency leads to significant attenuation. Finally, exploring the trends of
 455 transmission loss in either single incidence angle or diffuse field shows that
 456 the locally resonant nature of the plate bring additional attenuation in the
 457 coincidence region where the plate is known to be acoustically transparent.

458 3. Acoustic radiation - Finite case

459 The previous designs \mathcal{R}_1^∞ and \mathcal{R}_2^∞ are supplemented by finite dimensions
 460 $L_x = L_y = 0.7$ m, and are denoted \mathcal{R}_1 and \mathcal{R}_2 . \mathcal{R}_1 has $n_x = n_y = 8$ cells, \mathcal{R}_2
 461 has $n_x = n_y = 7$ cells. For explanatory purposes and in order to demonstrate
 462 the effect of locally resonant nature of the plate on the sound transmission
 463 loss, the simply supported case is chosen since it offers an analytical solution
 464 in the form of a double summation of sine terms. The location of point force
 465 and observation point for calculation of structural response are sketched in
 466 Fig. 2. From this setup, structural frequency response functions are assessed
 467 in section 3.1, then mean square velocity is commented in section 3.2. The
 468 behaviors identified make it possible to better understand the shape of the
 469 transmission loss curve in section 3.3.

470 3.1. Comparison of Timoshenko and homogenized model

471 This section briefly presents the structural response of the orthogonally
 472 ribbed plate modeled either with Timoshenko equation Eq. (1) or homog-

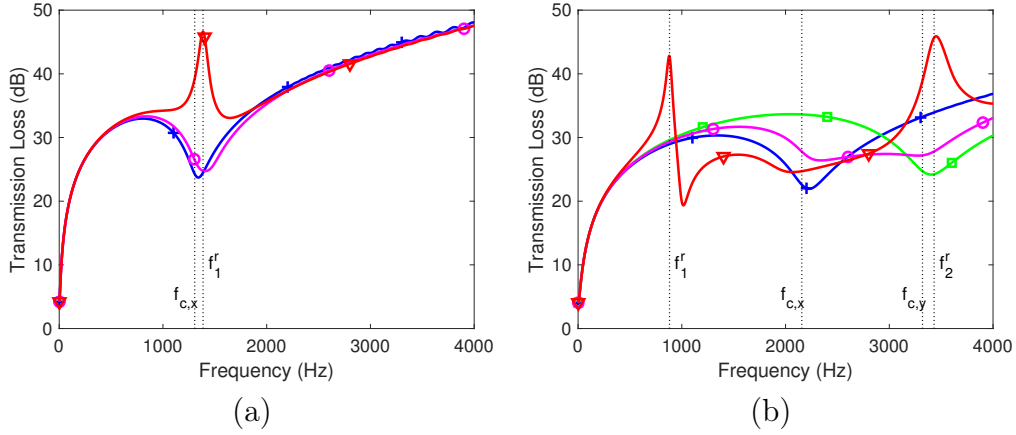


Figure 8: Diffuse field transmission loss of orthotropic plate with inner resonance ($-\triangle-$), plate at rest ($-\circ-$), equivalent isotropic plate in x - direction ($-\oplus-$) and y - direction ($-\square-$). For plate \mathcal{R}_1^∞ (a) and plate \mathcal{R}_2^∞ (b).

473 enized model with inner resonance Eq. (11). For this purpose, a struc-
 474 tural point force is located at coordinates $x_F = (L_x/2, L_y/2)$ and the trans-
 475 verse velocity is calculated at a virtual observation point with coordinates
 476 $x_v = (L_x/3, L_y/3)$. In this way, the structural frequency response func-
 477 tion defined as the ratio of velocity versus input force, namely mobility
 478 $M(\omega) = i\omega u/F$, is calculated analytically. For the sake of simplicity,
 479 plates with simply supported boundary conditions all around are consid-
 480 ered since there are distinct solutions for the wavenumbers k_x and k_y and
 481 it provides an analytical solution. The solution for the transverse displace-
 482 ment field $u(x, y, \omega)$ is formulated as the infinite sum of all possible solutions
 483 $u(x, y, \omega) = \sum_{m=1}^{\infty} \sum_{n=1}^{\infty} u_{m,n}(\omega) \Psi_{m,n}(x, y)$, where $\Psi_{m,n}(x, y)$ is the (m, n)
 484 mode shape function and $w_{m,n}(\omega)$ the associated amplitude. In case of a
 485 plate supported along all four edges, the modal functions are $\Psi_{m,n}(x, y) =$
 486 $\sin(m\pi x/L_x) \sin(n\pi y/L_y)$. This modal summation technique can be approx-
 487 imated as a finite sum as $u(x, y, \omega) \approx \sum_{m=1}^M \sum_{n=1}^N u_{m,n}(\omega) \Psi_{m,n}(x, y)$, where
 488 M and N are the number of modes considered. Considering 50 modes, the
 489 computational time is about 4 seconds and associated results are given for
 490 both designs on Fig. 9. The structural mobility is calculated as

491

492 Apart from the inner resonance frequencies specific to each design, the
 493 very low frequency behavior is well captured by the homogenized model, as
 494 well as the trend in rather high frequency domain. In addition, the response

495 from homogenized model exhibits proper drops of amplitude at the frequen-
 496 cies identified as inner resonance frequencies, which makes it possible to rely
 497 on its ability to predict local phenomena.

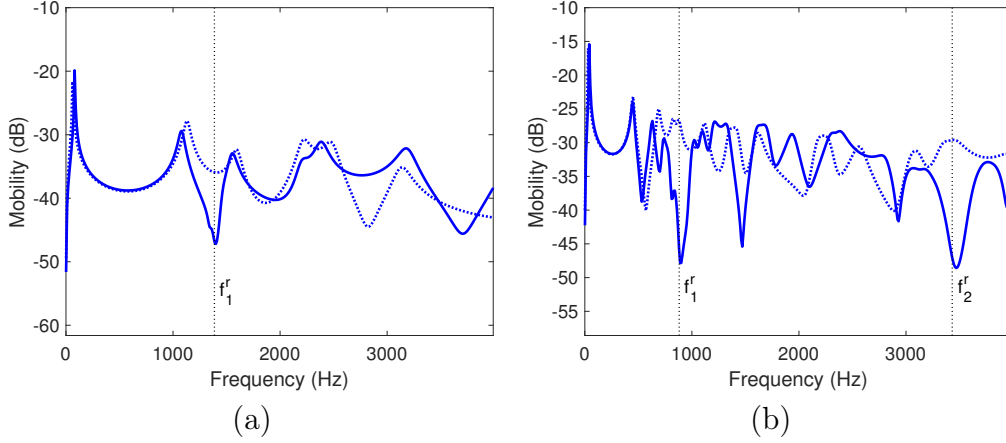


Figure 9: Structural mobility (ref:1m/s/N) of simply supported orthotropic plate with inner resonance computed analytically from homogenized model (—) and Timoshenko model (⋯). For plate \mathcal{R}_1 (a) and plate \mathcal{R}_2 (b).

498 3.2. Effect on mean square velocity

499 The mean square velocity is a structural indicator of the radiation per-
 500 formance, it is defined as the quadratic normal component of the structural
 501 velocity integrated over the surface of the plate S as $\tilde{v} = \sqrt{1/S \int_S |i\omega u|^2}$.
 502 The mean square velocity is calculated from this expression for both designs
 503 with same location of excitation point as in the previous section 3.1.

504 As illustrated in Fig. 10, the global modes are correctly predicted by the
 505 two models, especially in the low frequency region. However, strong disparity
 506 appears around the inner resonance frequencies, and the homogenized model
 507 shows better capability in predicting the gap induced by local resonance.
 508 Indeed, it is derived as a beam grid enriched by local motion of internal
 509 plates. As contrast between beam grid and plate constituents increases, the
 510 amplitude of motion experienced by internal plates becomes much different
 511 than that of the beam grid, leading to a poorer accuracy of Timoshenko
 512 model and giving advantage to the homogenized model.

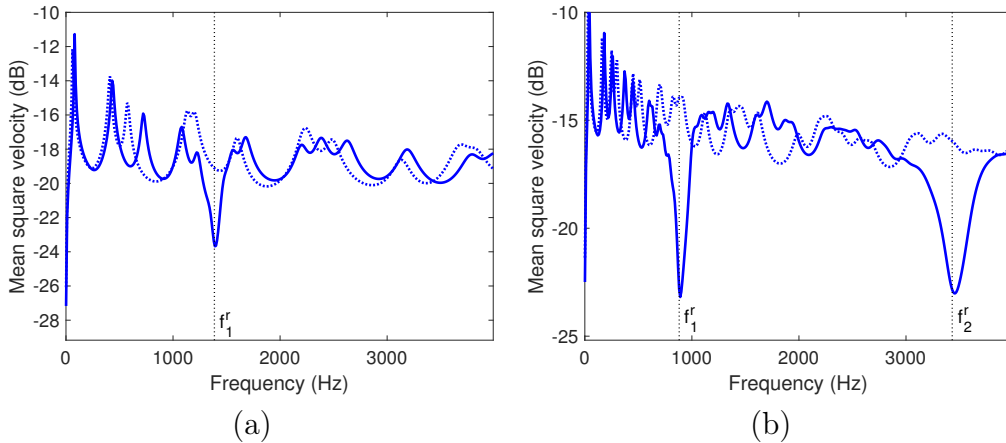


Figure 10: Mean square velocity (ref:1m/s/N) of orthotropic plate with inner resonance computed analytically from homogenized model (—) and Timoshenko model (···). For plate \mathcal{R}_1 (a) and plate \mathcal{R}_2 (b).

513 3.3. Effect on transmission loss

514 The transmission loss is here investigated by supplementing the previous
 515 model with simply supported plate. As for the structural part, the input
 516 vibratory field is the the same as the one calculated in section 3.1. As for the
 517 acoustic part, the notations are indicated in Fig. 2. The Rayleigh integral
 518 is implemented as it is known to be an efficient basis to calculate sound
 519 radiation from finite sized plane surface set into an infinite rigid baffle. The
 520 infinite baffle simplifies the general Helmholtz formulation so that only one
 521 integral is left, and the acoustic pressure is :

$$p(\mathbf{r}, \omega) = \frac{j\omega\rho}{2\pi} \iint_S \frac{v_n(\mathbf{r}_S) \exp(-ikR)}{R} dS \quad (23)$$

522 where $v_n(\mathbf{r}_S)$ is the normal velocity field over the surface, k is the acoustic
 523 wavenumber and $R = \|\mathbf{r}_S - \mathbf{r}\| = \sqrt{(x - x')^2 + (y - y')^2 + z'^2}$ is the distance
 524 between each elementary source point on the plate $\mathbf{r}_S = (x, y, 0)$ and the re-
 525 ceiver point $\mathbf{r} = (x', y', z')$. The sources are defined by subdividing the plate
 526 into a regular grid of 100×100 elementary sources. For the calculation of
 527 transmission loss, $z' \ll 1$.

528

529 The results in terms of sound transmission loss are represented in Fig. 11.
 530 Since our phenomenon occurs in a narrow interval, the choice is made not
 531 to adopt the classical representation in third octave bands. For both plates,

532 we see that inner resonance introduces additional loss in the sound trans-
533 mission To best emphasize the locally resonant feature, it is compared as in
534 Fig. 10 with the Timoshenko model to show the interval of differences. The
535 homogenized model is also used with internal plates at rest, which does not
536 correspond to a physical case but associated with a asymptotic behavior.

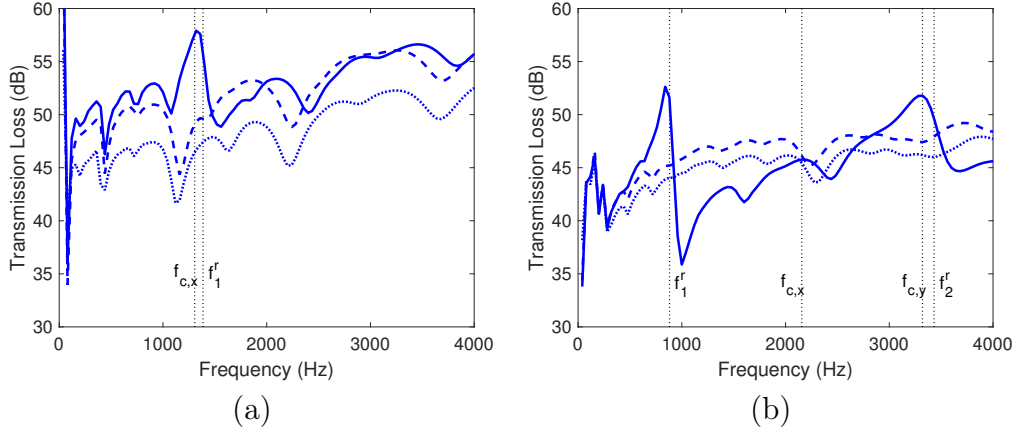


Figure 11: Transmission loss estimated analytically in case of finite plate, from homoge-
nized model with resonant plates ($-$), homogenized with plates at rest ($- -$), and from
Timoshenko model ($\cdot\cdot\cdot$). For plate \mathcal{R}_1 (a) and plate \mathcal{R}_2 (b).

537 Conclusion

538 Based on explicit design rules and homogenized plate model, this paper
539 brings phenomenological interpretation on the radiation of ribbed plates, and
540 specifically focuses on the parallel between an homogenized analytical model
541 of contrasted ribbed and its acoustic radiation compared to the Timoshenko
542 orthotropic plate model. For ribbed plates with strong contrasts between
543 constituents, it is firstly demonstrated that this model supplements Timo-
544 shenko model. The latter is suitable for ribbed plates in which the rigidity
545 of the plate is introduced in the bending stiffness of the ribs, whereas the
546 homogenized model can be seen as a beam grid whose dynamic behavior is
547 corrected by the motion of vibrating internal plates. Investigations of the
548 acoustic radiation from an infinite and finite orthogonally ribbed plate are
549 based on two designs associated with strong and low contrast between con-
550 stituents, in order to better exhibit the orthotropic nature of the plate.

551 As a preliminary comprehensive study case, the infinite plate case is pre-
552 sented. The limit behavior of equivalent isotropic plates in the two directions
553 of orthotropy are successfully identified. The radiation efficiency exhibits the
554 transition from non-radiating to radiating domains marked out by the criti-
555 cal frequency. The effect of the local resonance is also evidenced and results
556 in an unconventional increase or reduction of the radiation below or above
557 the critical frequency.

558 As a complementary case, analytical predictions of mean square veloc-
559 ity and transmission loss are commented for finite plates. It comes out that
560 the homogenized provides enhanced estimation of behavior in inner frequency
561 ranges compared to Timoshenko model. The examination of the sound trans-
562 mission loss demonstrates the attenuation in the neighborhood of inner res-
563 onance.

564 Although the homogenization process could be further applied on various
565 cell geometries, this paper specifically outlines the relevancy of the homog-
566 enized model and demonstrates its ability to predict acoustic radiation of
567 contrasted plates. The large amount of possible setups suggest adjustable
568 resonant properties of the panel behavior, and offers the possibility of either
569 broadband or narrow band attenuation.

570 **CRedit author statement**

571 **Pascal Fossat:** Conceptualization, Methodology, Software, Writing -
572 original draft, Writing - review & editing. **Thomas Brion:** Methodology,
573 Software, Writing - review & editing. **Mohamed Ichchou:** Conceptualiza-
574 tion, Writing - review & editing, Validation, Project administration, Funding
575 acquisition. **Olivier Bareille:** Supervision, Project administration, Funding
576 acquisition.

577 **Acknowledgments**

578 This work was supported by the LabEx CeLyA (Centre Lyonnais d'
579 Acoustique, ANR-10-LABX-0060) of Université de Lyon, within the program
580 “Investissements d’Avenir” (ANR-11-IDEX-0007) operated by the French Na-
581 tional Research Agency (ANR).

582 **References**

- 583 [1] P. W. Smith, Coupling of sound and panel vibration below the
584 critical frequency, *The Journal of the Acoustical Society of Amer-*
585 *ica* 36 (8) (1964) 1516–1520. arXiv:[https://doi.org/10.1121/1.](https://doi.org/10.1121/1.1919235)
586 [1919235](https://doi.org/10.1121/1.1919235), doi:[10.1121/1.1919235](https://doi.org/10.1121/1.1919235).
587 URL <https://doi.org/10.1121/1.1919235>
- 588 [2] N. Lomas, S. Hayek, Vibration and acoustic radiation of elastically sup-
589 ported rectangular plates, *Journal of Sound and Vibration* 52 (1) (1977)
590 1–25. doi:[https://doi.org/10.1016/0022-460X\(77\)90385-6](https://doi.org/10.1016/0022-460X(77)90385-6).
591 URL [https://www.sciencedirect.com/science/article/pii/](https://www.sciencedirect.com/science/article/pii/S0022460X77903856)
592 [0022460X77903856](https://www.sciencedirect.com/science/article/pii/S0022460X77903856)
- 593 [3] A. Berry, J. Nicolas, Structural acoustics and vibration be-
594 havior of complex panels, *Applied Acoustics* 43 (3) (1994)
595 185–215, *structural Acoustics and Vibrations*. doi:[https://doi.org/10.1016/0003-682X\(94\)90047-7](https://doi.org/10.1016/0003-682X(94)90047-7).
596 URL [https://www.sciencedirect.com/science/article/pii/](https://www.sciencedirect.com/science/article/pii/S0003682X94900477)
597 [0003682X94900477](https://www.sciencedirect.com/science/article/pii/S0003682X94900477)
- 599 [4] N. Atalla, R. Bernhard, Review of numerical solutions for
600 low-frequency structural-acoustic problems, *Applied Acoustics*
601 43 (3) (1994) 271–294, *structural Acoustics and Vibrations*.
602 doi:[https://doi.org/10.1016/0003-682X\(94\)90050-7](https://doi.org/10.1016/0003-682X(94)90050-7).
603 URL [https://www.sciencedirect.com/science/article/pii/](https://www.sciencedirect.com/science/article/pii/S0003682X94900507)
604 [0003682X94900507](https://www.sciencedirect.com/science/article/pii/S0003682X94900507)
- 605 [5] E. Reynders, C. Van Hoorickx, A. Dijckmans, Sound transmission
606 through finite rib-stiffened and orthotropic plates, *Acta Acustica united*
607 *with Acustica* 102 (6) (2016) 999–1010. doi:[https://doi.org/10.](https://doi.org/10.3813/AAA.919015)
608 [3813/AAA.919015](https://doi.org/10.3813/AAA.919015).
- 609 [6] C. Decraene, G. Lombaert, E. P. Reynders, Prediction of diffuse sound
610 transmission through finite-sized periodic structures, *Journal of Sound*
611 *and Vibration* 528 (2022) 116851. doi:[https://doi.org/10.1016/j.](https://doi.org/10.1016/j.jsv.2022.116851)
612 [jsv.2022.116851](https://doi.org/10.1016/j.jsv.2022.116851).
- 613 [7] S. Timoshenko, S. Woinowsky-Krieger, *Theory of Plates and Shells*, En-
614 *gineering mechanics series*, McGraw-Hill, 1959.

- 615 [8] G. Maidanik, Response of ribbed panels to reverberant acoustic fields,
616 The Journal of the Acoustical Society of America 34 (6) (1962) 809–
617 826. arXiv:<https://doi.org/10.1121/1.1918200>, doi:10.1121/1.
618 1918200.
619 URL <https://doi.org/10.1121/1.1918200>
- 620 [9] D. Crighton, G. Maidanik, Acoustic and vibration fields generated
621 by ribs on a fluid-loaded panel, I: Plane-wave problems for a sin-
622 gle rib, Journal of Sound and Vibration 75 (3) (1981) 437–452.
623 doi:[https://doi.org/10.1016/0022-460X\(81\)90388-6](https://doi.org/10.1016/0022-460X(81)90388-6).
624 URL [https://www.sciencedirect.com/science/article/pii/
625 0022460X81903886](https://www.sciencedirect.com/science/article/pii/0022460X81903886)
- 626 [10] B. Mace, Sound radiation from a plate reinforced by two sets of parallel
627 stiffeners, Journal of Sound and Vibration 71 (3) (1980) 435–441.
628 doi:[https://doi.org/10.1016/0022-460X\(80\)90425-3](https://doi.org/10.1016/0022-460X(80)90425-3).
629 URL [https://www.sciencedirect.com/science/article/pii/
630 0022460X80904253](https://www.sciencedirect.com/science/article/pii/0022460X80904253)
- 631 [11] D. Mead, Y. Yaman, The harmonic response of rectangular
632 sandwich plates with multiple stiffening: A flexural wave anal-
633 ysis, Journal of Sound and Vibration 145 (3) (1991) 409–428.
634 doi:[https://doi.org/10.1016/0022-460X\(91\)90111-V](https://doi.org/10.1016/0022-460X(91)90111-V).
635 URL [https://www.sciencedirect.com/science/article/pii/
636 0022460X9190111V](https://www.sciencedirect.com/science/article/pii/0022460X9190111V)
- 637 [12] D. Mead, A general theory of harmonic wave propagation
638 in linear periodic systems with multiple coupling, Journal of
639 Sound and Vibration 27 (2) (1973) 235–260. doi:[https://doi.org/10.1016/0022-460X\(73\)90064-3](https://doi.org/10.1016/0022-460X(73)90064-3).
640 URL [https://www.sciencedirect.com/science/article/pii/
641 0022460X73900643](https://www.sciencedirect.com/science/article/pii/0022460X73900643)
- 643 [13] J.-L. Christen, M. Ichchou, A. Zine, B. Troclet, Wave finite element
644 formulation of the acoustic transmission through complex infinite plates,
645 Acta Acustica united with Acustica 102 (6) (2016) 984–991. doi:<https://doi.org/10.3813/AAA.919013>.
646
- 647 [14] C. Droz, C. Zhou, M. Ichchou, J.-P. Lainé, A hybrid wave-
648 mode formulation for the vibro-acoustic analysis of 2D periodic

- 649 structures, *Journal of Sound and Vibration* 363 (2016) 285–302.
650 doi:<https://doi.org/10.1016/j.jsv.2015.11.003>.
651 URL [https://www.sciencedirect.com/science/article/pii/](https://www.sciencedirect.com/science/article/pii/S0022460X15008779)
652 [S0022460X15008779](https://www.sciencedirect.com/science/article/pii/S0022460X15008779)
- 653 [15] F. Fahy, E. Lindqvist, Wave propagation in damped, stiff-
654 ened structures characteristic of ship construction, *Journal of*
655 *Sound and Vibration* 45 (1) (1976) 115–138. doi:[https://doi.org/10.1016/0022-460X\(76\)90671-4](https://doi.org/10.1016/0022-460X(76)90671-4).
656 URL [https://www.sciencedirect.com/science/article/pii/](https://www.sciencedirect.com/science/article/pii/0022460X76906714)
657 [0022460X76906714](https://www.sciencedirect.com/science/article/pii/0022460X76906714)
- 659 [16] J. Legault, A. Mejdj, N. Atalla, Vibro-acoustic response of or-
660 thogonally stiffened panels: The effects of finite dimensions,
661 *Journal of Sound and Vibration* 330 (24) (2011) 5928–5948.
662 doi:<https://doi.org/10.1016/j.jsv.2011.07.017>.
663 URL [https://www.sciencedirect.com/science/article/pii/](https://www.sciencedirect.com/science/article/pii/S0022460X11005852)
664 [S0022460X11005852](https://www.sciencedirect.com/science/article/pii/S0022460X11005852)
- 665 [17] H. Zhou, Y. Zhao, H. Wu, J. Meng, The vibroacoustic analysis of
666 periodic structure-stiffened plates, *Journal of Sound and Vibration* 481
667 (2020) 115402. doi:<https://doi.org/10.1016/j.jsv.2020.115402>.
668 URL [https://www.sciencedirect.com/science/article/pii/](https://www.sciencedirect.com/science/article/pii/S0022460X20302340)
669 [S0022460X20302340](https://www.sciencedirect.com/science/article/pii/S0022460X20302340)
- 670 [18] E. Sánchez-Palencia, Non-homogeneous media and vibration theory,
671 *Lecture notes in physics* 127.
- 672 [19] C. Chesnais, C. Boutin, S. Hans, Effects of the local resonance on
673 the wave propagation in periodic frame structures: Generalized new-
674 tonian mechanics, *The Journal of the Acoustical Society of Amer-*
675 *ica* 132 (4) (2012) 2873–2886. arXiv:[https://doi.org/10.1121/1.](https://doi.org/10.1121/1.4744975)
676 [4744975](https://doi.org/10.1121/1.4744975), doi:[10.1121/1.4744975](https://doi.org/10.1121/1.4744975).
677 URL <https://doi.org/10.1121/1.4744975>
- 678 [20] C. Boutin, K. Viverge, Generalized plate model for highly contrasted
679 laminates, *European Journal of Mechanics - A/Solids* 55 (2016) 149–
680 166. doi:<https://doi.org/10.1016/j.euromechsol.2015.08.008>.
681 URL [https://www.sciencedirect.com/science/article/pii/](https://www.sciencedirect.com/science/article/pii/S0997753815001084)
682 [S0997753815001084](https://www.sciencedirect.com/science/article/pii/S0997753815001084)

- 683 [21] K. Viverge, C. Boutin, F. Sallet, Model of highly contrasted
684 plates versus experiments on laminated glass, *International*
685 *Journal of Solids and Structures* 102-103 (2016) 238–258.
686 doi:<https://doi.org/10.1016/j.ijsolstr.2016.09.035>.
687 URL [https://www.sciencedirect.com/science/article/pii/](https://www.sciencedirect.com/science/article/pii/S0020768316302840)
688 [S0020768316302840](https://www.sciencedirect.com/science/article/pii/S0020768316302840)
- 689 [22] P. Fossat, C. Boutin, M. Ichchou, Dynamics of periodic ribbed plates
690 with inner resonance: Analytical homogenized model and dispersion
691 features, *International Journal of Solids and Structures* 152-153 (2018)
692 85–103. doi:<https://doi.org/10.1016/j.ijsolstr.2018.06.012>.
693 URL [https://www.sciencedirect.com/science/article/pii/](https://www.sciencedirect.com/science/article/pii/S0020768318302440)
694 [S0020768318302440](https://www.sciencedirect.com/science/article/pii/S0020768318302440)
- 695 [23] C. Boutin, P. Fossat, C. Droz, M. Ichchou, Dynamics of ribbed plates
696 with inner resonance: Analytical homogenized models and experimental
697 validation, *European Journal of Mechanics - A/Solids* 79 (2020) 103838.
698 doi:<https://doi.org/10.1016/j.euromechsol.2019.103838>.
699 URL [https://www.sciencedirect.com/science/article/pii/](https://www.sciencedirect.com/science/article/pii/S0997753819301664)
700 [S0997753819301664](https://www.sciencedirect.com/science/article/pii/S0997753819301664)
- 701 [24] P. Fossat, M. Ichchou, Sound radiation of locally resonant unidirection-
702 ally ribbed plates, in: *ASME 2021 International Mechanical Engineering*
703 *Congress and Exposition*, Vol. 85543, American Society of Mechanical
704 Engineers, 2021. arXiv:[https://asmedigitalcollection.asme.](https://asmedigitalcollection.asme.org/IMECE/proceedings-pdf/IMECE2021/85543/V001T01A032/6826596/v001t01a032-imece2021-70987.pdf)
705 [org/IMECE/proceedings-pdf/IMECE2021/85543/V001T01A032/](https://asmedigitalcollection.asme.org/IMECE/proceedings-pdf/IMECE2021/85543/V001T01A032/6826596/v001t01a032-imece2021-70987.pdf)
706 [6826596/v001t01a032-imece2021-70987.pdf](https://asmedigitalcollection.asme.org/IMECE/proceedings-pdf/IMECE2021/85543/V001T01A032/6826596/v001t01a032-imece2021-70987.pdf), doi:10.1115/
707 [IMECE2021-70987](https://doi.org/10.1115/IMECE2021-70987).
708 URL <https://doi.org/10.1115/IMECE2021-70987>
- 709 [25] Z. Liu, R. Rumpler, L. Feng, Broadband locally resonant meta-
710 material sandwich plate for improved noise insulation in the
711 coincidence region, *Composite Structures* 200 (2018) 165–172.
712 doi:<https://doi.org/10.1016/j.compstruct.2018.05.033>.
713 URL [https://www.sciencedirect.com/science/article/pii/](https://www.sciencedirect.com/science/article/pii/S0263822318303520)
714 [S0263822318303520](https://www.sciencedirect.com/science/article/pii/S0263822318303520)
- 715 [26] T. Yamamoto, Acoustic metamaterial plate embedded with helmholtz
716 resonators for extraordinary sound transmission loss, *Journal of Applied*

- 717 Physics 123 (21) (2018) 215110. arXiv:[https://doi.org/10.1063/1.](https://doi.org/10.1063/1.5025570)
718 [5025570](https://doi.org/10.1063/1.5025570), doi:[10.1063/1.5025570](https://doi.org/10.1063/1.5025570).
719 URL <https://doi.org/10.1063/1.5025570>
- 720 [27] C. Droz, O. Robin, M. Ichchou, N. Atalla, Improving sound transmis-
721 sion loss at ring frequency of a curved panel using tunable 3D-printed
722 small-scale resonators, *The Journal of the Acoustical Society of Amer-*
723 *ica* 145 (1) (2019) EL72–EL78. arXiv:[https://doi.org/10.1121/1.](https://doi.org/10.1121/1.5088036)
724 [5088036](https://doi.org/10.1121/1.5088036), doi:[10.1121/1.5088036](https://doi.org/10.1121/1.5088036).
725 URL <https://doi.org/10.1121/1.5088036>
- 726 [28] F. Errico, M. Ichchou, S. De Rosa, F. Franco, O. Bareille, In-
727 vestigations about periodic design for broadband increased sound
728 transmission loss of sandwich panels using 3D-printed models,
729 *Mechanical Systems and Signal Processing* 136 (2020) 106432.
730 doi:<https://doi.org/10.1016/j.ymssp.2019.106432>.
731 URL [https://www.sciencedirect.com/science/article/pii/](https://www.sciencedirect.com/science/article/pii/S0888327019306533)
732 [S0888327019306533](https://www.sciencedirect.com/science/article/pii/S0888327019306533)